Palaeogeography, Palaeoclimatology, Palaeoecology 451 (2016) 152–163

Contents lists available at ScienceDirect

Palaeogeography, Palaeoclimatology, Palaeoecology

journal homepage: www.elsevier.com/locate/palaeo

Sulfur isotope constraints on marine transgression in the lacustrine Upper Cretaceous Songliao Basin, northeastern China

Hansheng Cao [a], Alan J. Kaufman [b,*], Xuanlong Shan [a,*], Huan Cui [c], Guijie Zhang [d]

[a] College of Earth Sciences, Jilin University, Changchun 130061, China
[b] Department of Geology and Earth System Science Interdisciplinary Center, University of Maryland, College Park, MD 20742-4211, United States
[c] Department of Geology, University of Maryland, College Park, MD 20742-4211, United States
[d] CAS Key Laboratory of Crust–Mantle Materials and Environments, School of Earth and Space Sciences, University of Science and Technology of China, Hefei 230026, China

ARTICLE INFO

Article history:
Received 6 April 2015
Received in revised form 8 February 2016
Accepted 23 February 2016
Available online 2 March 2016

Keywords:
Songliao Basin
Nenjiang Formation
Santonian
Campanian
Transgression
C/S
Carbon isotope
Sulfur isotope

ABSTRACT

Organic-rich Cretaceous source rocks of the petroliferous Songliao Basin in northeast China are considered to be lacustrine in origin, but paleontological and organic geochemical evidence suggest episodic marine incursions. As a test of this hypothesis, we applied time-series measurements of elemental and isotopic abundances on core and cutting samples to evaluate fluctuations in the sulfur and carbon cycles across the Santonian–Campanian transition preserved in the upper Yaojia and lower Nenjiang formations. The data reveal a spike in pyrite sulfur abundance and a marked negative excursion in $\delta^{34}S$ at the base of the Nenjiang Formation when the basin expanded to its maximal extent. The elemental and isotopic data suggest that flooding was associated with rapid marine transgression that enhanced sulfate concentrations, which promoted microbial sulfate reduction in anoxic bottom waters that were episodically euxinic. Subsequent restriction of the basin and a decline in marine influence is supported by progressive upsection ^{34}S enrichment (up to 30‰) in Nenjiang Member I, which are interpreted to reflect the distillation of sulfate through enhanced pyrite burial, followed by a gradual return to lacustrine conditions that prevailed in overlying strata.

1. Introduction

The Cretaceous Period is generally characterized by hothouse climates and repeated oceanic anoxic events (OAEs) resulting in the deposition of organic-rich source rocks in marine environments and associated positive carbon and sulfur isotope anomalies (Tarduno et al., 1998; Skelton et al., 2003; Owens et al., 2013). The OAEs may be linked to the reorganization of ocean circulation patterns and enhanced greenhouse gas concentrations in the atmosphere, which were potentially enhanced by widespread rifting and volcanism (Arthur et al., 1990; Poulsen et al., 2001). At present, however, it is unclear whether the globally distributed marine events may have teleconnections to the terrestrial realm through either atmospheric processes or oceanic transgression onto continental margins.

To evaluate whether the continental Upper Cretaceous Songliao Basin of northeast China was influenced by ocean water and evaluate redox conditions during the deposition of important source rocks, we conducted a high-resolution time-series carbon and sulfur isotope study of the Santonian to Campanian Yaojia and Nenjiang formations. The sedimentary rocks of the Songliao Basin contain the most productive oil and gas reserves of the country, and are widely believed to be lacustrine in origin due to the preservation of terrestrial and freshwater plant and animals fossils (Wu et al., 2007; Sha, 2007; Feng et al., 2010; Wan et al., 2013). On the other hand, a marine affinity for source rocks of both the Qingshankou and lower Nenjiang formations is supported by the discovery of foraminifera (Xi et al., 2011), euryhaline dinoflagellates (Hou et al., 2000), and fish adapted to saline environments, as well as the preservation of specific organic biomarkers, including certain methyl- and desmethylsteranes, gammacerane, and β-carotene (Song et al., 2013). If correct, OAE expression in the lacustrine Songliao Basin is likely related to episodic marine transgression (Arthur and Sageman, 2005) conceivably linked to enhanced seafloor spreading and global warming.

The third and last of the Cretaceous OAEs (Wagreich, 2012) around the Coniacian–Santonian boundary (which is restricted to equatorial to mid-latitude Atlantic and adjacent basins, but not including the north or south Atlantic nor the Tethys or Pacific oceans) coincides with a nadir of $^{87}Sr/^{86}Sr$ values recorded in marine proxies. This observation suggests that enhanced hydrothermal circulation associated with greater ridge activity (Jones and Jenkyns, 2001) could explain marine transgression, as well as increasing temperature through volcanic release of CO_2 (Royer, 2006). Insofar as ridge volume provides a first-order control on eustatic sea level, it is plausible that the lacustrine Songliao Basin was episodically flooded in response to global tectonic activity during the Cretaceous Period. Marine flooding (in particular

* Corresponding authors.
E-mail addresses: kaufman@umd.edu (A.J. Kaufman), shanxl@jlu.edu.cn (X. Shan).

http://dx.doi.org/10.1016/j.palaeo.2016.02.041
0031-0182/

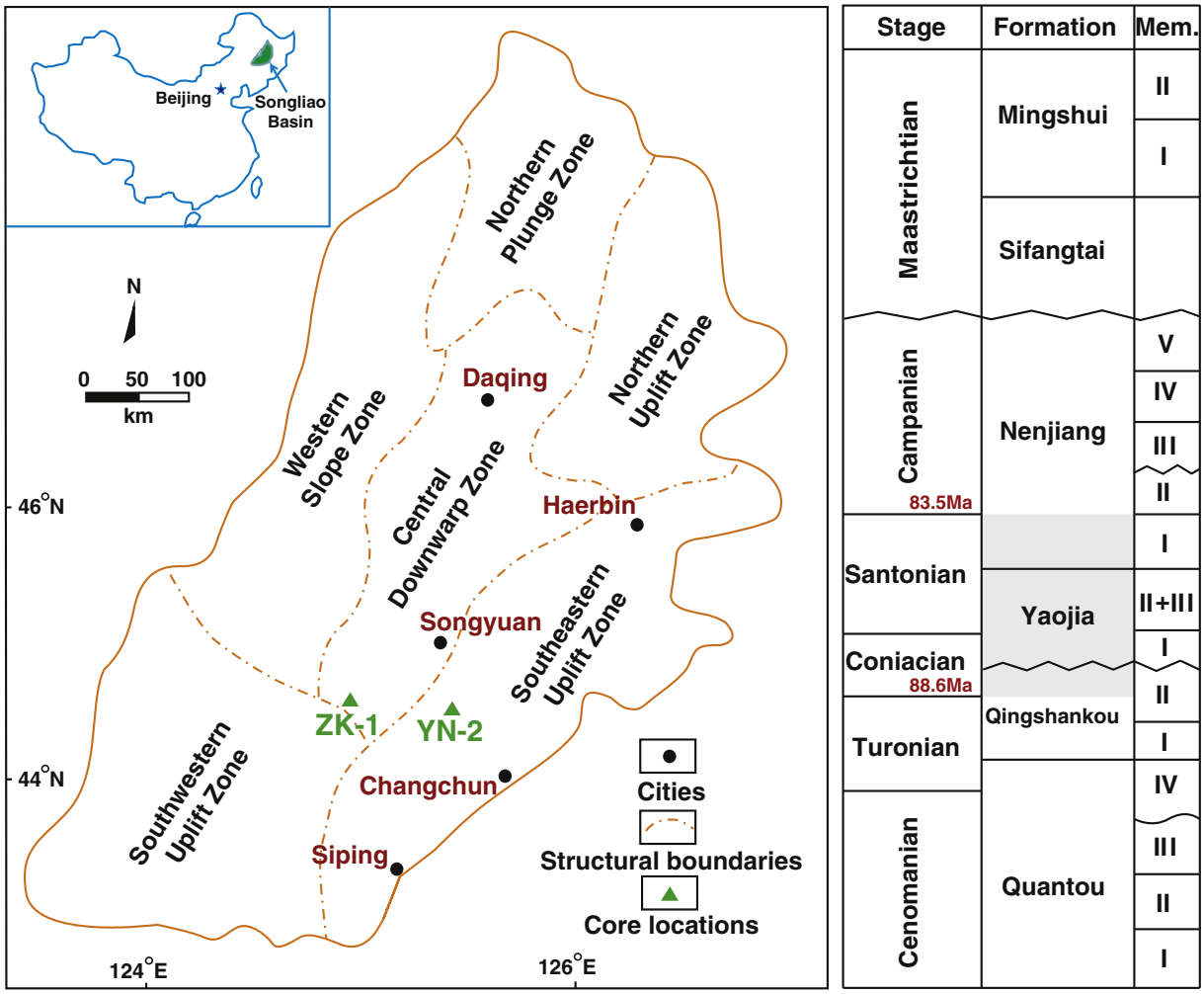

Fig. 1. Map of structural units with locations of cores used in this study (YN-2 and ZK-1) along with Late Cretaceous stage assignments for units in the Songliao Basin of Northeast China (modified from Feng et al., 2010). Grey interval spanning from the upper Qingshankou to the lower Nenjiang formations broadly corresponds to OAE 3 (ca. 88.6–83.5 Ma) in the marine realm (Wagreich, 2012).

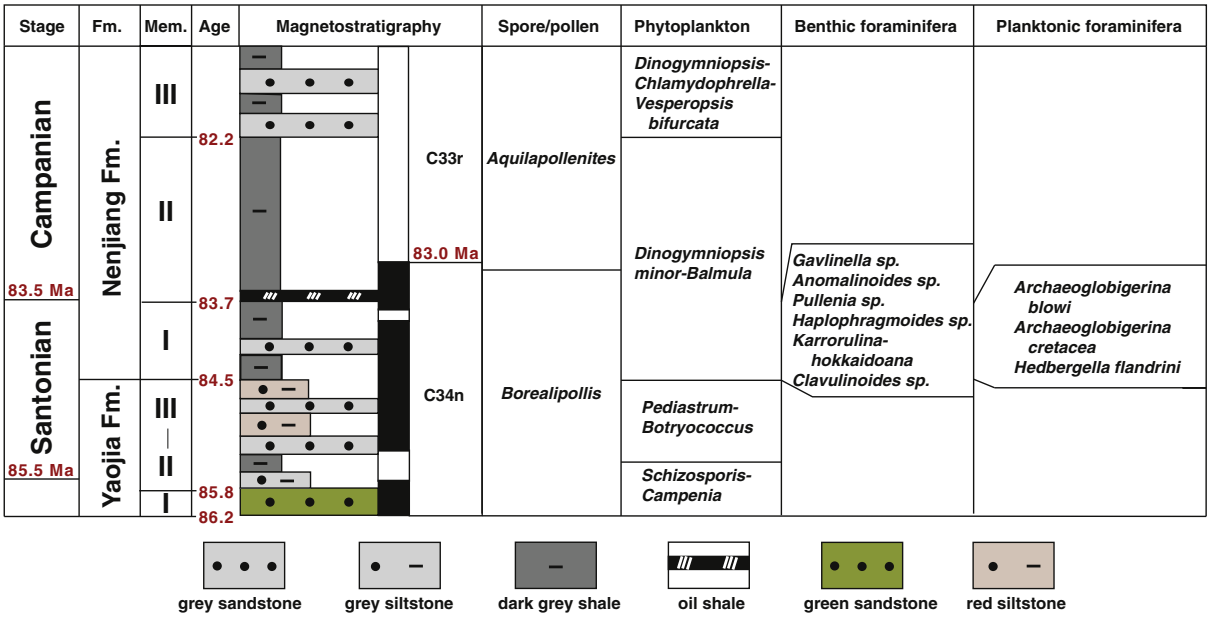

Fig. 2. Lithostratigraphy, magnetostratigraphy, and biostratigraphy of the Yaojia and lower Nenjiang formations (modified from Wan et al., 2013; Xi et al., 2011).

Table 1
Solvent leaching experimental results.

Name	TOC (%)	TOC average	TOC deviation	δ^{13}Corg (‰, VPDB)	δ^{13}C average	δ^{13}C deviation
YN1830N1	2.44			−29.62		
YN1830N2	2.74	2.72		−29.62	−29.59	
YN1830N3	2.99		0.60	−29.52		−0.51
YN1830D1	1.98			−29.21		
YN1830D2	2.01	1.92		−29.05	−29.07	
YN1830D3	1.77			−28.96		
YN1798N1	5.83			−28.69		
YN1798N2	4.73	5.38		−28.76	−28.69	
YN1798N3	5.59		0.95	−28.64		−0.13
YN1798D1	4.46			−28.45		
YN1798D2	4.37	4.43		−28.54	−28.56	
YN1798D3	4.45			−28.70		
YN1744N1	1.31			−26.77		
YN1744N2	1.40	1.37		−26.77	−26.72	
YN1744N3	1.41		0.03	−26.63		−0.11
YN1744D1	1.21			−26.72		
YN1744D2	1.42	1.34		−26.67	−26.61	
YN1744D3	1.40			−26.43		
YN1852N1	2.13			−28.70		
YN1852N2	1.79	1.91		−28.78	−28.75	
YN1852N3	1.82		0.66	−28.77		−0.02
YN1852D1	1.27			−28.70		
YN1852D2	1.32	1.25		−28.71	−28.73	
YN1852D3	1.15			−28.77		
YN1884N1	0.24			−26.36		
YN1884N2	0.29	0.23		−26.30	−26.35	
YN1884N3	0.15		−0.04	−26.39		0.15
YN1884D1	0.22			−26.27		
YN1884D2	0.26	0.27		−26.72	−26.50	
YN1884D3	0.32			−26.52		
Average			0.44			−0.13

during the deposition of the Qingshankou and lower Nenjiang formations) would have enhanced salinity and increased sulfate levels. Seawater incursions and upwelling of nutrient-rich bottom waters may have also promoted high rates of primary productivity, eutrophication and widespread anoxia in the basin, which are tested in this time-series elemental and sulfur isotope study of core and cuttings from exploration wells.

2. Geological setting

2.1. Tectonic evolution and sequence stratigraphy of the Songliao Basin

The Songliao Basin located northeast of Beijing in China is one of the largest Cretaceous-aged intra-cratonic sedimentary rift basins in the world (Fig. 1). It experienced four episodes of deformation spanning from the Late Jurassic to the Cenozoic, including: (1) mantle upwelling and doming, (2) rifting, (3) thermal subsidence, and (4) structural inversion (Feng et al., 2010). The basin is characterized by six structural units, which are believed to control the distribution of source reservoirs, including oil and natural gas, shale gas, and oil sands.

Approximately 10 km of Jurassic through Neogene clastic deposits in-fill the basin, but most strata are of Jurassic and Cretaceous age. Mesozoic strata of the Songliao Basin are divided into nine unconformity-bounded sequences. The first three of these, represented by the upper Jurassic Huoshiling Formation and lower Cretaceous Shahezi and Yingchengzi formations, include volcanics as well as clastic rocks associated with coarse-grained alluvial fans and fine-grained playa lakes that accumulated during rifting (Zhou and Littke, 1999). Thermal subsidence then resulted in the initiation of lacustrine sedimentation, which is believed to have begun around 155 Ma (Wang et al., 2013a) in the Denglouku Formation and continued across four major unconformities to near the top of the Cretaceous section, including the Quantuo, Qingshantuo, Yaojia, and Nenjiang formations (Feng et al., 2010). An unconformity within the Nenjiang Formation likely marks the first of several Cretaceous compressional events that induced basin inversion and progressive coarsening of sediments in the upper Nenjiang, Sifangtai, and Mingshui formations.

2.2. Lake expansion and marine transgression

Exploration drill holes throughout the Songliao Basin reveal that the extent of the freshwater "lake" expanded considerably during the accumulation of the organic-rich Qingshankuo (Turonian and Coniacian stages) and Nenjiang (Santonian and Campanian stages) formations (Gao et al., 1992; Zhou and Littke, 1999; Feng et al., 2010). However, the basal organic-rich mudstone in Member I of the Qingshankou contains numerous dolomite horizons that are consistent with increasing salinity associated with marine transgression. Support for this view comes from the observation of a monospecific *Triangulicypristorsuosus* ostracode assemblage with low numbers of genera and species (Wan et al., 2013), which have been attributed to an oligohaline to mesohaline depositional environment (Xi et al., 2011).

An environment with similar salinity is interpreted for the low diversity *Cyprideaanonyma–Candonafabiforma* assemblage in the basal Nenjiang Formation Member I, as well as the depauperate *Cyprideagracila–Cyprideagunsulinensis* assemblage in the upper part of the member. Notably, both benthic and planktonic foraminifera of Upper Cretaceous marine origin have also been identified in Nenjiang Members I and II (Xi et al., 2011). Insofar as ostracodes and foraminifera are sensitive to a range of ecological factors, including salinity, temperature, and chemical composition (Holmes and Chivas, 2002; Ye et al., 2002; Gao et al., 2008), the Nenjiang paleontological data supports a

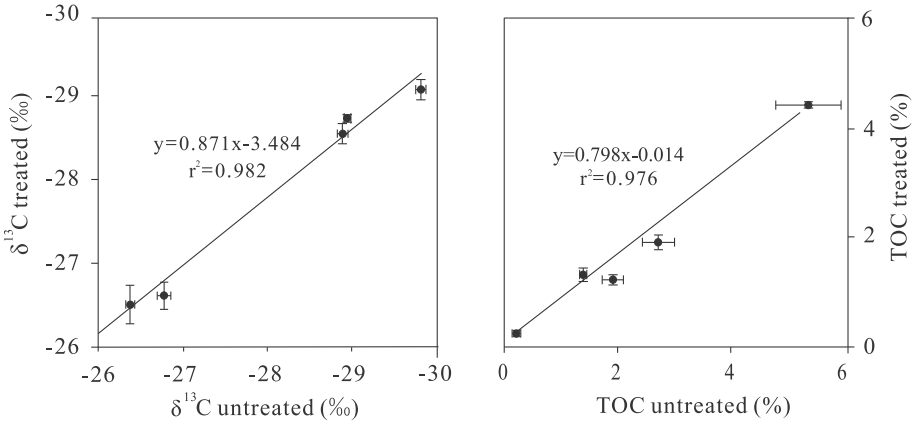

Fig. 3. Statistical comparison of total organic carbon (TOC) abundances and carbon isotope (δ^{13}C) compositions based on triplicate analyses of treated and untreated cutting samples used in the leaching experiments.

marine incursion during Member I. Independent evidence for salinity (and redox) stratification of the lower Nenjiang water column are interpreted from biomarker studies (Sinninghe-Damasté et al., 1995; Grice et al., 1998; Sinninghe-Damasté et al., 1993; Barakat and Rullkötter, 1997; Jia et al., 2013; Bechtel et al., 2012; Song et al., 2013).

2.3. The Yaojia and Nenjiang formations

The Yaojia and Nenjiang formations include siliciclastic-dominated facies that are commonly attributed to fluvial, deltaic, and lacustrine depositional environments (Fig. 2). The Yaojia is subdivided into three members (total thickness ranging from 80 to 210 m) and the Nenjiang into five (100–470 m total thickness). Grey to black shale in Members I and II of the Nenjiang Formation accumulated in the deepest environments during the maximal extent of the basin; the oil shale at the boundary between the two members is considered an important marker horizon. A U–Pb SIMS age of bentonite within the lower Nenjiang oil shale horizon of ~83.7 Ma (Deng et al., 2013) places it very near to the Santonian–Campanian boundary (ca. 85.5 Ma). The boundary is broadly coincident with the end of the Cretaceous Normal Superchron (C34), which lasted nearly 40 million years (from 121 to 83 Ma), and the beginning of the C33 interval (from 83 to 79 Ma) of rapid reversed magnetic polarity (Granot et al., 2012; Wan et al., 2013). In Members I and II of the Nenjiang Formation, sedimentation and organic carbon burial rates have been estimated at ~20 cm/kyr and 1.89 Tg/yr (Ye et al., 2002; Wang et al., 2013b). Rock eval measurements reveal that most of the organic matter in Nenjiang Member I and the lower portion of Member II is hydrogen-rich (Type I) produced by aquatic photosynthetic organisms (Jia et al., 2013; Bechtel et al., 2012), including algae and dinoflagellates. However, Type III organic matter of terrestrial origin becomes increasingly abundant through upper Member II and into Member III. An angular unconformity separates Members II and III of the Nenjiang Formation (Feng et al., 2010); grey, green, and red shale and siltstone, as well as white sandstone characterize Member III, which accumulated in dominantly fluvial and lacustrine environments as the basin decreased in size and depth.

3. Materials and methods

Samples were taken from boreholes YN-2 and ZK-1, located approximately 200 km apart in the Central Downwarp and Southeastern Uplift regions, respectively (Fig.1). The ZK-1 core reached a total depth of ~500 m and intersected the Nenjiang, Sifangtai, and Mingshui formations. Core samples from ZK-1 were previously collected for a study of oil shale resource potential, and thus focused on the most organic-rich specimens, especially those around the Nenjiang Member I/II boundary. In contrast, the cutting samples from the YN-2 core were systematically collected every two meters through the upper Yaojia and lower Nenjiang formations for time-series analyses.

To evaluate whether the core and cutting samples (which were previously washed and crushed at Jilin University) were contaminated by drilling fluids or migrated oil, chips from five uncrushed cutting samples from a nearby core that intersected the Nenjiang Formation were selected for solvent extraction. Approximately 10 g of sample were placed into 50 ml tubes and leached with 20 ml of pure dichloromethane (DCM) (2×, 5 h each) in order to remove soluble organic matter from chip surfaces. After the second leach step, the chips were sonicated for 20 min with Milli-Q (18 MΩ) water, soaked for an hour (2×), and then decanted in order to remove residual DCM. Leached cutting samples were then dried at 80 °C overnight and then crushed (200 mesh) in a ceramic ring-and-puck mill cleaned between samples with baked quartz sand. Bulk crushed powders prepared at either Jilin University or University of Maryland were weighed and then repeatedly acidified with 3 M HCl to quantitatively remove carbonate. The residues, including siliciclastic grains, pyrite, and organic matter, were then washed with Milli-Q water until solutions reached neutral pH prior to drying in an 80 °C oven overnight. The dried residues were quantified in order to calculate % carbonate in the bulk samples; aliquots of between 0.5 and 5 mg were weighed into tin cups for organic carbon and pyrite sulfur (with V_2O_5 as an additional oxidant) determinations.

The sulfur abundance and isotopic composition of pyrite (assuming elemental S is negligible in these samples) were measured by combustion to SO_2 with a Eurovector elemental analyzer in-line with a second Eurovector Isoprime isotope ratio mass spectrometer (IRMS). The tin cups were sequentially dropped with a pulsed O_2 purge of 12 ml into a quartz column packed with high purity reduced copper wire and heated to 1040 °C, as well as a $Mg(ClO_4)_2$ desiccant column to remove water. The SO_2 was separated from other gases with a 3-m stainless steel GC column packed with Porapak-Q heated to 60 °C. Timed pulses of SO_2 reference gas (Airgas 99.999% purity, ~6 nA) were introduced at the beginning of the run using an injector connected to the IRMS with a fixed open ratio split. The isotope ratios of reference and sample peaks were determined by monitoring ion beam intensities relative to background values. Isotopic results are expressed in the delta notation as per mil (‰) deviations from the Canyon Diablo (V-CDT) standard. Two NBS-127 standards and two NZ-1 standards were measured between each set of 10 samples, and uncertainties for each analytical session based on these standard analyses were better than 1.0% and 0.3‰, respectively, for abundance and isotope compositions. Total sulfur contents of bulk samples were calculated by quantifying IRMS SO_2 peak areas relative to those from measured amounts of standard materials and the % carbonate.

Measurements for organic carbon abundance and isotope composition were similar to those of sulfur, except that the quartz reaction column was packed with chromium oxide and silvered cobaltous/cobaltic oxide and heated to 1040 °C. The analyte also flowed through a second column at 1040 °C packed with high purity reduced copper wire for quantitative reduction of NO_2 and N_2O and O_2 resorption, as well as a $Mg(ClO_4)_2$ desiccant column to remove water. The CO_2 was separated from other gases with a 3-m stainless steel GC column packed with Porapak-Q heated to 60 °C. Timed pulses of CO_2 reference gas (Airgas 99.999% purity, ~6 nA) were introduced at the beginning of the run using an injector connected to the IRMS with a fixed open ratio split. The isotope ratios of reference and sample peaks were determined by monitoring ion beam intensities relative to background values. The cycle time for these analyses was 430 s with reference gas injection as two a 30-s pulse beginning at 15 and 60 s. Sample CO_2 peaks begin at 200 s and return to baseline around 240 s. Two urea standards were measured between each set of 10 samples and uncertainties for each analytical session based on these standard analyses were determined to be better than 1.0% and 0.1‰, respectively, for abundance and carbon isotope composition. Total organic carbon contents were calculated by quantifying the % carbonate in the bulk samples and IRMS CO_2 peak areas relative to those from measured amounts of urea standards.

4. Results

Results of our solvent leaching study are presented in Table 1 and Fig. 3, while those of the time-series carbonate, total organic carbon (TOC) abundance and isotope composition, and pyrite sulfur abundance and isotope composition from the YN-2 and ZK-1 cores are presented in Tables 2 and 3 and illustrated in Figs. 4 and 5.

4.1. Leaching experiments

In the solvent extraction study, cutting samples were split with half remaining untreated as a control and the other half sequentially leached with DCM and washed with Milli-Q water. Although the leaching experiments showed no apparent change in the color of the solvent between treatments, after crushing and acidification the residues of leached and unleached cutting samples did reveal small statistical differences in

Table 2
Carbon and sulfur abundance and isotope compositions of Upper Cretaceous Nenjiang and Yaojia member samples from the YN-2 core.

Layer	Depth (m)	Stage	$CaCO_3$ (%)	TOC (%)	δ^{13}Corg (‰, VPDB)	TS (%)	δ^{34}S (‰, VCDT)	TOC/TS
Nenjiang Member III	1688	Campanian	15.14	0.91	−26.74	0.38	6.72	2.39
	1690	Campanian	17.14	0.51	−26.56	0.37	5.35	1.38
	1692	Campanian	14.65	1.35	−25.81	0.33	5.45	4.09
	1694	Campanian	14.49	0.98	−26.59	0.34	6.66	2.88
	1696	Campanian	18.88	0.67	−27.62	0.79	9.64	0.85
	1698	Campanian	15.19	1.15	−26.97	0.40	7.07	2.88
	1700	Campanian	16.39	1.60	−26.87	0.33	6.41	4.85
	1702	Campanian	5.87	1.05	−26.50	0.33	5.60	3.18
	1704	Campanian	11.22	0.87	−26.68	0.35	3.61	2.49
	1706	Campanian	16.28	0.94	−26.90	0.34	6.09	2.76
	Average		14.53	1.00	−26.72	0.40	6.26	2.78
	stdev		3.64	0.31	0.45	0.14	1.55	1.16
Nenjiang Member II	1708	Campanian	19.62	0.95	−27.03	0.43	6.40	2.21
	1710	Campanian	14.42	1.08	−27.02	0.31	5.67	3.48
	1712	Campanian	12.64	1.14	−27.26	0.38	7.57	3.00
	1714	Campanian	15.98	1.01	−27.27	0.32	7.18	3.16
	1716	Campanian	17.51	0.91	−27.06	0.29	7.91	3.14
	1718	Campanian	16.70	1.08	−26.80	0.37	5.12	2.92
	1720	Campanian	14.55	1.49	−26.96	0.45	4.70	3.31
	1722	Campanian	12.65	1.75	−26.82	0.45	6.48	3.89
	1724	Campanian	9.39	2.33	−26.38	0.41	7.19	5.68
	1726	Campanian	12.46	1.96	−27.19	0.54	8.23	3.63
	1728	Campanian	14.45	2.09	−27.25	0.57	9.90	3.67
	1730	Campanian	14.72	1.67	−27.64	0.88	10.90	1.90
	1732	Campanian	11.80	2.05	−28.14	0.82	10.33	2.50
	1734	Campanian	12.71	1.42	−28.40	0.66	8.73	2.15
	1736	Campanian	16.42	0.89	−27.68	0.39	5.36	2.28
	1738	Campanian	16.16	1.38	−27.75	0.43	10.45	3.21
	1740	Campanian	14.60	1.41	−27.83	0.44	11.73	3.20
	1742	Campanian	13.49	1.52	−27.71	0.58	12.00	2.62
	1744	Campanian	11.95	1.45	−28.73	1.41	10.09	1.03
	1746	Campanian	−8.05	1.87	−28.29	1.60	12.96	1.17
	1748	Campanian	10.47	1.46	−28.55	1.51	11.20	0.97
	1750	Campanian	12.55	1.77	−28.57	1.01	11.23	1.75
	1752	Campanian	10.91	1.67	−28.77	1.13	11.87	1.48
	1754	Campanian	11.09	1.73	−28.83	1.44	12.14	1.20
	1756	Campanian	12.80	1.93	−28.58	0.92	11.48	2.10
	1758	Campanian	9.96	3.31	−29.68	0.40	8.07	8.28
	1760	Campanian	11.99	2.67	−29.35	0.78	12.54	3.42
	1762	Campanian	12.14	0.80	−29.40	0.91	12.07	0.88
	1764	Campanian	8.39	2.54	−29.64	0.97	12.31	2.62
	1766	Campanian	8.27	3.01	−29.41	1.13	12.82	2.66
	1768	Campanian	10.15	1.38	−28.96	0.71	13.25	1.94
	1770	Campanian	9.98	3.80	−29.40	0.91	11.86	4.18
	1772	Campanian	15.72	4.14	−28.79	0.73	12.13	5.67
	1774	Campanian	8.74	5.92	−29.45	0.98	15.27	6.04
	1776	Campanian	9.89	6.46	−28.97	1.49	8.02	4.34
	1778	Campanian	14.29	5.52	−29.62	0.99	13.56	5.58
	1780	Campanian	13.24			0.97	15.50	
	1782	Campanian	17.05	3.87	−29.77	0.91	14.80	4.25
	1784	Campanian	25.01	3.75	−30.80	0.77	17.83	4.87
	1786	Campanian	19.67	3.31	−29.35	0.95	12.70	3.48
	1788	Campanian	20.84	3.02	−31.53	0.76	18.14	3.97
	1790	Campanian	23.62	3.27	−30.64	0.70	15.23	4.67
	1792	Campanian	17.97	2.18	−30.91	0.69	17.02	3.16
	1794	Campanian	17.37	3.56	−31.27	0.84	17.40	4.24
	1796	Campanian	22.96	2.56	−30.97	0.50	18.30	5.12
	1798	Campanian	19.16	3.05	−30.45	0.69	17.19	4.42
	1800	Campanian	20.94	2.82	−31.51	0.59	17.15	4.78
	1802	Campanian	21.45	2.34	−30.18	0.59	15.44	3.97
	1804	Campanian	20.80	2.44	−30.14	0.34	15.74	7.18
	Average		14.32	2.37	−28.81	0.76	11.66	3.44
	stdev		5.35	1.30	1.40	0.34	3.79	1.61
Nenjiang Member I	1808	Campanian	19.64	1.09	−30.31	0.57	14.66	1.91
	1810	Campanian	15.34	1.64	−31.22	0.94	13.51	1.74
	1814	Campanian	16.07	4.65	−30.81	0.95	14.38	4.89
	1816	Campanian	15.35	3.81	−30.51	1.06	13.33	3.59
	1818	Campanian	15.57	5.03	−31.18	1.28	15.77	3.93
	1820	Campanian	31.16	3.33	−30.36	1.43	19.39	2.33
	1822	Campanian	19.39	2.98	−30.57	2.17	16.39	1.37
	1824	Santonian	16.48	1.65	−30.46	2.15	15.79	0.77
	1826	Santonian	17.21	1.49	−29.91	1.96	16.93	0.76
	1828	Santonian	17.32	1.25	−29.50	3.85	16.95	0.32
	1830	Santonian	16.93	0.81	−28.92	1.64	18.10	0.49
	1832	Santonian	18.34	0.77	−29.38	3.25	24.23	0.24

Table 2 (*continued*)

Layer	Depth (m)	Stage	$CaCO_3$ (%)	TOC (%)	δ^{13}Corg (‰, VPDB)	TS (%)	δ^{34}S (‰, VCDT)	TOC/TS
Nenjiang Member I	1834	Santonian	14.75	1.57	−29.39	3.13	24.54	0.50
	1836	Santonian	17.30	0.74	−29.47	3.35	22.17	0.22
	1838	Santonian	11.21	2.38	−29.17	1.39	3.08	1.71
	1840	Santonian	13.08	1.00	−29.42	2.86	10.35	0.35
	1842	Santonian	13.14	1.52	−28.62	2.20	7.19	0.69
	1844	Santonian	16.35	2.13	−28.83	2.44	10.22	0.87
	1846	Santonian	16.12	2.14	−29.90	1.44	9.81	1.49
	1848	Santonian	15.56	1.25	−29.36	5.57	−4.05	0.22
	1850	Santonian	19.12	0.86	−28.73	2.46	−4.93	0.35
	Average		16.93	2.00	−29.81	2.19	13.23	1.37
	stdev		3.88	1.27	0.79	1.18	7.88	1.33
Yaojia Member III	1852	Santonian	19.54	0.66	−28.67	2.03	1.13	0.33
	1854	Santonian	17.94	1.63	−29.32	1.04	5.58	1.57
	1856	Santonian	19.02	0.72	−28.36	1.06	2.31	0.68
	1858	Santonian	17.14	0.39	−28.51	0.63	7.09	0.62
	1860	Santonian	21.40	0.42	−28.79	0.77	10.40	0.55
	1862	Santonian	21.65	0.70	−28.37	0.40	6.71	1.75
	1864	Santonian	19.97	0.44	−28.74	0.53	6.44	0.83
	1866	Santonian	18.19	0.34	−28.11	0.36	6.95	0.94
	1868	Santonian	17.75	0.96	−29.53	0.31	2.24	3.10
	1870	Santonian	20.40	0.48	−27.88	0.47	8.72	1.02
	Average		19.30	0.67	−28.63	0.76	5.76	1.14
	stdev		1.56	0.39	0.51	0.52	2.99	0.82

both TOC and ^{13}C abundances (Fig. 3). For the TOC analyses, the paired measurements were highly correlated ($r^2 = 0.976$), but the slope of the relationship indicated that the treated samples had ~20% less organic matter than untreated samples. The largest difference was noted in the most organic-rich specimen. For the δ^{13}C measurements, the paired analyses were also highly correlated ($r^2 = 0.982$). In this case, the slope of this relationship suggests that treated samples are enriched in ^{13}C by ~13% relative to the untreated specimens, but the paired offsets are small considering the ‰ scale of deviations.

4.2. Chemostratigraphy

The carbonate abundance in the Nenjiang Formation in the ZK-1 core (Fig. 5) is variable, ranging from 10% to 40%, with no clear stratigraphic trend. However, in the cutting samples from YN-2 (Fig. 4) the % carbonate reveals much less short-term variability, with values around 18% in samples from the Yaojia through Nenjiang Member I with a step-wise drop to near 10% at the base of Nenjiang Member II followed by a gradual increase back to nearly 18% at the top of the sampled interval. Total organic carbon (TOC) contents in both cores are highest at the base of Nenjiang Member II (especially at the base of ZK-1 where concentrations are as high as 8.7%). This organic-rich horizon is a marker bed throughout the Songliao Basin, and notably coincides with the step-wise drop in carbonate abundance recorded in the YN-2 core cuttings. A smaller secondary TOC peak is preserved in Member I from samples of both cores. The carbon isotope compositions of TOC in the YN-2 core define a well-defined negative excursion that starts in the Yaojia with values around −27‰ and falls to a nadir of ca. −32‰ just below the Nenjiang Member I/II boundary before rising monotonically to −26‰ at the base of Nenjiang Member III. The rising limb of the δ^{13}C excursion is reproduced in Nenjiang Member II data from the ZK-1 core samples, but the falling limb is more difficult to discern given the lack of systematic sampling in Member I from that core.

In the YN-2 core, the total sulfur content of samples (not including acid-volatile and carbonate-associated sulfate that would be removed during acidification) is greatest in Nenjiang Member I (with concentrations up to 5.6%) relative to the Yaojia and Nenjiang Members II and III. The progressive upsection increase in total sulfur abundances in the lower half of Member I is notably coincident with an initial 15‰ drop in δ^{34}S values followed by a 30‰ positive excursion (Fig. 4). Across the Member I/II boundary and through the overlying 110 m of Member II, the δ^{34}S values of samples monotonically decline from as high as +25‰ to a low of ca. +8‰. In contrast, extremely high sulfur abundances were determined from samples selected for the resource potential study of the ZK-1 core in both Nenjiang Members I and III, and there appears to be two δ^{34}S anomalies: one at the base of Member I that is strikingly similar in trend and magnitude to the excursion recorded in YN-2, and a second at the base of Member II associated with very high TOC abundances of the samples (Fig. 5).

5. Discussion

5.1. Preservation of organic matter

Concerns regarding potential organic contamination of core samples and cuttings from drilling fluids and/or migrated oil prompted an initial extraction study on five uncrushed cutting samples from a nearby core that intersected the Nenjiang Formation. The results indicated a statistical 20% difference in TOC abundance between treated and untreated samples (Fig. 3), but it is uncertain whether this relates to the leaching of indigenous soluble organic matter, or to the potential organic contaminants. Pertinent to this issue, the δ^{13}C analyses of the treated and untreated residues reveal only minor isotopic contrasts, with most being less than 0.5‰. The coincidence of paired isotope values gives us confidence that the time-series trends in δ^{13}C from untreated rock powders faithfully record depositional conditions. If correct, it is most likely that the statistically lower TOC abundances of treated samples reflect the leaching of solvent-extractable indigenous organic matter, rather than the loss of admixed drilling fluids or of migrated oil.

5.2. Redox consequences of marine transgression

Marine transgression, which would have flooded the lacustrine Songliao Basin with seawater sulfate and other salts, appears to be the most parsimonious explanation for the published paleontological observations and organic biomarker results from the basal Nenjiang Formation. With enhanced sulfate concentrations, sulfide could have built up in pore waters, as well as the deeper water column, through microbial sulfate reduction (MSR); if ferrous iron were available on the surfaces of mineral grains or dissolved in anoxic solutions, highly insoluble pyrite would form. For example, in the deep anoxic Black Sea, high concentrations of dissolved hydrogen sulfide allows pyrite to form in the water column, which then rains down and accumulates in the sediments (Hirst, 1974; Berner and Raiswell, 1983; Wilkin and Arthur, 2001; Schenau et al., 2002; Schoonen, 2004; Huang et al., 2013).

Table 3
Carbon and sulfur abundance and isotope compositions of Upper Cretaceous Nenjiang and Yaojia member samples from the ZK-1 core.

Layer	Depth (m)	Stage	$CaCO_3$ (%)	TOC (%)	δ^{13}Corg (‰, VPDB)	TS (%)	δ^{34}S (‰, VCDT)	TOC/TS
Nenjiang Member III	197.63	Campanian	9.50	0.10	−25.50	0.24		0.42
	203.75	Campanian	8.67	0.51	−25.73	0.50	6.17	1.02
	207.36	Campanian	13.86	0.22	−26.24	0.15	−2.45	1.47
	216.1	Campanian	15.93	0.12	−27.27	2.96	2.90	0.04
	233.9	Campanian	9.01	0.35	−25.48	0.57	3.74	0.61
	236.55	Campanian	11.83	0.24	−27.04	0.45	12.71	0.53
	237.95	Campanian	9.85	0.39	−26.49	1.58	18.45	0.25
	240.15	Campanian	13.07	0.55	−27.77	0.28	1.16	1.96
	241.75	Campanian	12.77	0.34	−26.60	0.07	1.44	4.86
	242.15	Campanian	7.09	0.77	−27.62	0.05	12.44	15.40
	256.13	Campanian	10.20	1.04	−25.87	0.05	11.74	20.80
	260.92	Campanian	11.53	0.33	−26.93	0.17	17.46	1.94
	Average		11.11	0.41	−26.54	0.59	10.44	4.11
	stdev		2.52	0.27	0.80	0.86	11.38	6.47
Nenjiang Member II	264.13	Campanian	9.91	0.58	−25.33	0.05	5.31	11.60
	265.12	Campanian	15.74	0.97	−27.55	0.32	11.53	3.03
	268.8	Campanian	9.66	9.29	−28.93	1.65	7.99	5.63
	272.35	Campanian	22.61	0.49	−27.17	0.03	9.98	16.33
	276.13	Campanian	12.23	0.74	−27.31	0.24	11.62	3.08
	278.03	Campanian	17.27	1.07	−28.04	0.24	9.30	4.46
	284.7	Campanian	17.20	0.82	−27.25	0.35	10.74	2.34
	300.8	Campanian	12.64	1.47	−27.31	0.10	5.73	14.70
	307.4	Campanian	10.99	1.86	−28.40	0.55	7.89	3.38
	312.4	Campanian	15.13	1.50	−27.38	0.45	13.40	3.33
	322.9	Campanian	31.40	1.04	−27.35	0.19	5.16	5.47
	320.75	Campanian	12.99	1.39	−26.38	0.09	4.52	15.44
	319.68	Campanian	15.28	1.24	−26.59	0.18	5.12	6.89
	318.61	Campanian	18.57	1.58	−27.00	0.19	4.09	8.32
	317.54	Campanian	18.22	1.54	−27.21	0.19	4.51	8.11
	316.47	Campanian	14.60	1.38	−27.35	0.25	5.17	5.52
	315.4	Campanian	18.25	0.86	−27.57	0.30	5.26	2.87
	323.93	Campanian	11.42	1.19	−27.32	0.28	5.06	4.25
	330.38	Campanian	18.54	1.39	−26.91	0.12	4.73	11.58
	338.9	Campanian	9.05	1.75	−26.97	0.25	7.36	7.00
	343.37	Campanian	34.49	1.07	−26.94	0.14	6.12	7.64
	360.12	Campanian	13.69	2.26	−27.87	0.16	7.56	14.13
	379.65	Campanian	10.97	1.19	−27.64	0.24	6.81	4.96
	391.1	Campanian	22.83	1.45	−27.56	0.34	7.37	4.26
	401.25	Campanian	9.69	3.57	−26.98	0.32	7.57	11.16
	407.58	Campanian	7.71	3.22	−27.12	0.42	9.08	7.67
	411.35	Campanian	8.61	3.31	−27.32	0.75	8.80	4.41
	412.85	Campanian	25.82	2.89	−28.72	0.70	10.90	4.13
	413.6	Campanian	45.01	1.10	−28.13	0.81	8.73	1.36
	418.68	Campanian	7.16	2.32	−29.17	1.30	14.34	1.78
	426.8	Campanian	8.63	3.65	−29.10	0.99	10.81	3.69
	432.05	Campanian	6.60	3.65	−29.19	0.93	15.99	3.92
	434	Campanian	23.21	2.89	−30.48	0.87	24.29	3.32
	435.05	Campanian	6.69	6.34	−28.10	1.22	11.16	5.20
	436.1	Campanian	6.47	0.78	−26.16	0.07	9.18	11.14
	436.1	Campanian	6.47	0.78		0.09	8.44	8.67
	437.15	Campanian	24.56	6.71	−28.85	1.49	9.06	4.50
	438.2	Campanian	15.01	8.74	−29.17	1.84	2.61	4.75
	439.25	Campanian	10.00	5.96	−25.57	0.72	5.69	8.28
	441.35	Campanian	7.51	5.74	−29.14	0.42	17.93	13.67
	441.5	Campanian	7.51	5.74		0.46	18.40	12.48
	Average		15.32	2.49	−27.66	0.50	8.67	6.94
	stdev		8.38	2.22	1.07	0.47	4.22	4.12
Nenjiang Member I	442.4	Santonian	7.90	7.07	−29.35	0.23	26.89	30.74
	444.63	Santonian	17.31	9.18	−31.45	1.96	23.37	4.68
	447.15	Santonian	37.86	0.56	−29.86	0.57	4.96	0.98
	460.85	Santonian	11.89	6.62	−29.61	1.26	0.25	5.25
	475.75	Santonian	15.94	6.06	−30.88	1.90	22.99	3.19
	485.42	Santonian	41.89	0.14	−25.63	4.85	14.22	0.03
	489.17	Santonian	26.20	2.16	−29.04	2.81	7.11	0.77
	493.46	Santonian	29.59	0.07	−26.71	1.47	−3.58	0.05
	493.47	Santonian	29.59	0.07		1.56	−3.86	0.04
	498.43	Santonian	21.76	0.08	−27.22	2.06	−3.27	0.04
	500.5	Santonian	18.85	0.08	−27.61	0.14	12.13	0.57
	500.51	Santonian	18.85	0.08		0.14	12.20	0.57
	Average		20.59	2.84	−28.74	1.36	9.65	3.91
	stdev		10.59	3.19	1.88	1.27	10.16	8.65

Geochemists thus often rely on the ratio of weight percent TOC to total sulfur (indicated as TS) as an indicator of bottom water oxygenation (Fig. 6), with the lowest values interpreted to reflect the presence of hydrogen sulfide (euxinic conditions) dissolved in sedimentary pore waters or the deep water column or both (Goldhaber and Kaplan, 1974; Berner, 1982, 1984; Berner and Raiswell, 1983; Leventhal,

1983; Wilkin and Arthur, 2001; Schenau et al., 2002; McKay and Longstaffe, 2003; Sachse et al., 2012; Prauss, 2015). The TOC/TS values in lower Nenjiang Member I (Figs. 4, 5, and 6) from the YN-2 core are systematically low, with most samples having values of <1, suggesting the likelihood of widespread euxinia in the interval associated with the marine incursion. The spread of euxinic conditions into the photic zone would have provided a necessary source of electrons for anoxygenic photoautotrophs and other sulfide oxidizing bacteria living along a shallow chemocline within the basin (Jia et al., 2013; Bechtel et al., 2012). The abundance of TOC (Type I) is relatively low in the interpreted euxinic interval (potentially related to active water column recycling through sulfate reduction), and the $\delta^{13}C$ values remain constant in comparison to values preserved in underlying sedimentary rocks of the Yaojia Formation, as well as the overlying organic-rich horizons of upper Nenjiang Member I. Hence, the marked enrichments in TS in the interpreted euxinic interval do not correlate with significant changes in the carbon cycle.

The step-function rise in TOC/TS in upper Nenjiang Member I from the YN-2 core suggests that the influence of seawater sulfate on the production of sulfide rapidly declined. This is plausibly related to sea level regression that isolated the lake from the marine reservoir, and the distillation of sulfate remaining in the lake through pyrite burial. Given the return to lower TOC/TS in the Nenjiang Member II interval between about 1750 and 1770 m in the core, a second marine transgression seems plausible. However, there is no clear change in sulfur isotope fractionation within this interval that would be predicted from a seawater incursion (see below). Furthermore, progressive freshening of the basin after the Santonian–Campanian boundary is interpreted from organic geochemical and biomarker studies of the Member II oil shale. These indicate the dominance of a monospecific algal community, higher Pr/Ph values, a lower gammacerane index, and higher MTTC ratios, which suggest that Nenjiang Member II accumulated beneath an oxidized water column with low salinity and high bioproductivity (Bechtel et al., 2012; Song et al., 2013).

In Nenjiang Member III in the ZK-1 core, which is composed of coarse sandstones and shales as opposed to the mudstones that dominate lower in the succession, both TOC and TS are relatively low and TOC/TS are highly variable. While several samples fall in the same field as those from lower Nenjiang Member I (Fig. 6), we suggest that these represent a change in the provenance of coarser siliciclastic sediments (Feng et al., 2010), rather than a return to euxinic conditions in the depositional basin.

5.3. Factors influencing sulfur isotope fractionation

Understanding how marine transgression might influence the direction and magnitude of biologically induced sulfur isotope fractionation require a detailed understanding of both the reductive and oxidative paths of the sulfur cycle. On the reductive side, the magnitude of kinetic sulfur isotope fractionation (ε_{SR}) during dissimilatory MSR (simplified as $2CH_2O + SO_4^{2-} \rightarrow HS^- + 2HCO_3^- + H^+$) is observed to correlate *directly* with extracellular sulfate concentrations—with experiments from pure cultures indicating maximal discrimination between ^{34}S and ^{32}S of 66‰ at high sulfate concentrations (Sim et al., 2011). While ε_{SR} may be suppressed at very low sulfate abundances (<200 μM; Habicht et al., 2002), recent studies of euxinic systems (Wortmann et al., 2001; Canfield et al., 2010; Nakagawa et al., 2012; Gomes and Hurtgen, 2013; Crowe et al., 2014) indicate that large kinetic fractionations are achievable by both isolated and natural populations of sulfate reducers. Furthermore, environmentally controlled experiments suggest that MSR-related fractionation could be strain-specific (Habicht et al., 2002, 2005; Sim et al., 2011; Leavitt et al., 2013; Bradley et al., 2015), or related to sulfate reduction rates that are dependent on

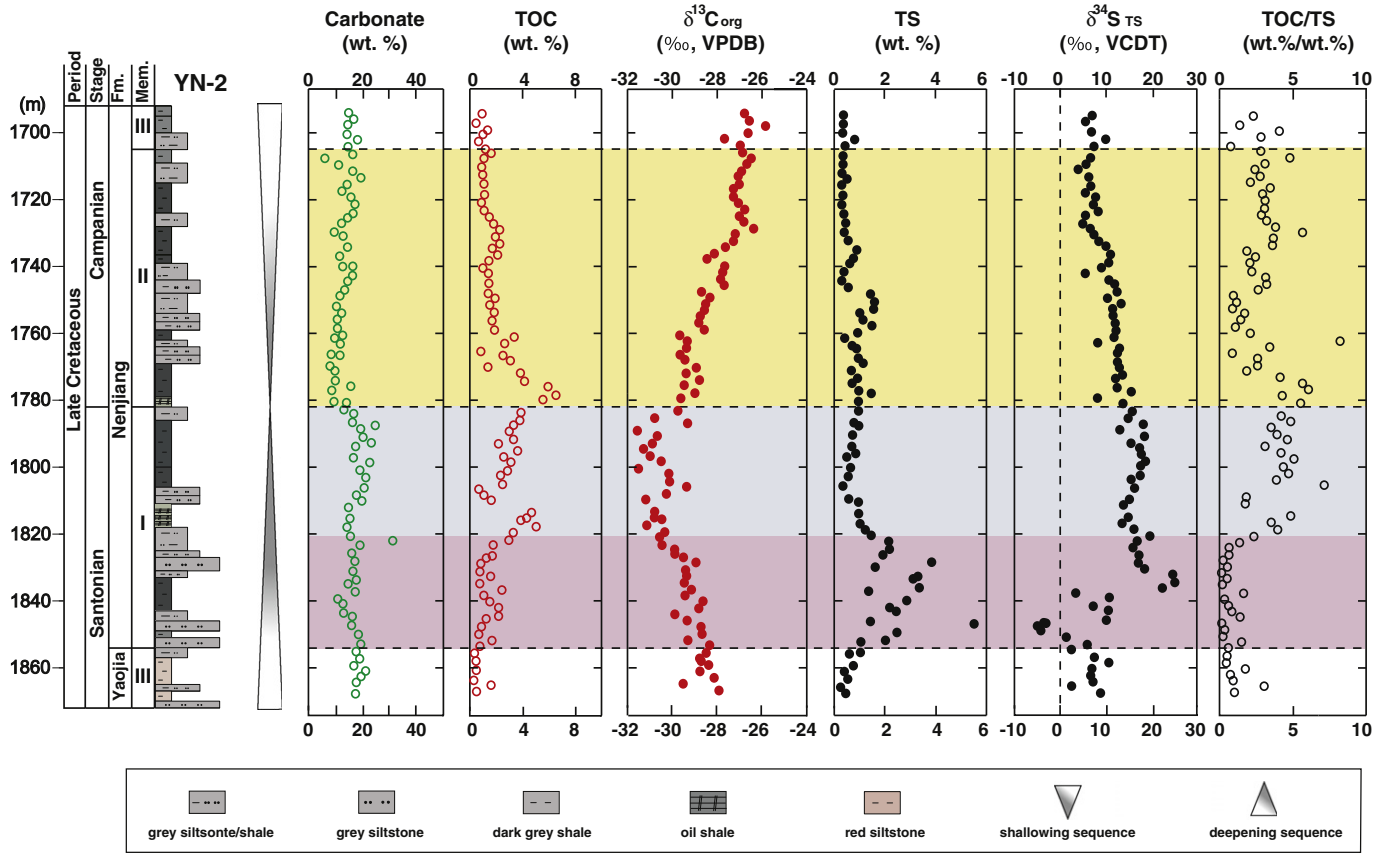

Fig. 4. Chemostratigraphy of YN-2 cutting samples from the Nenjiang and Yaojia formations of the Songliao Basin in northeastern China. The shaded intervals represent interpreted water column environmental conditions (purple = euxinic/stratified, blue = anoxic/stratified, and yellow = oxygenated).

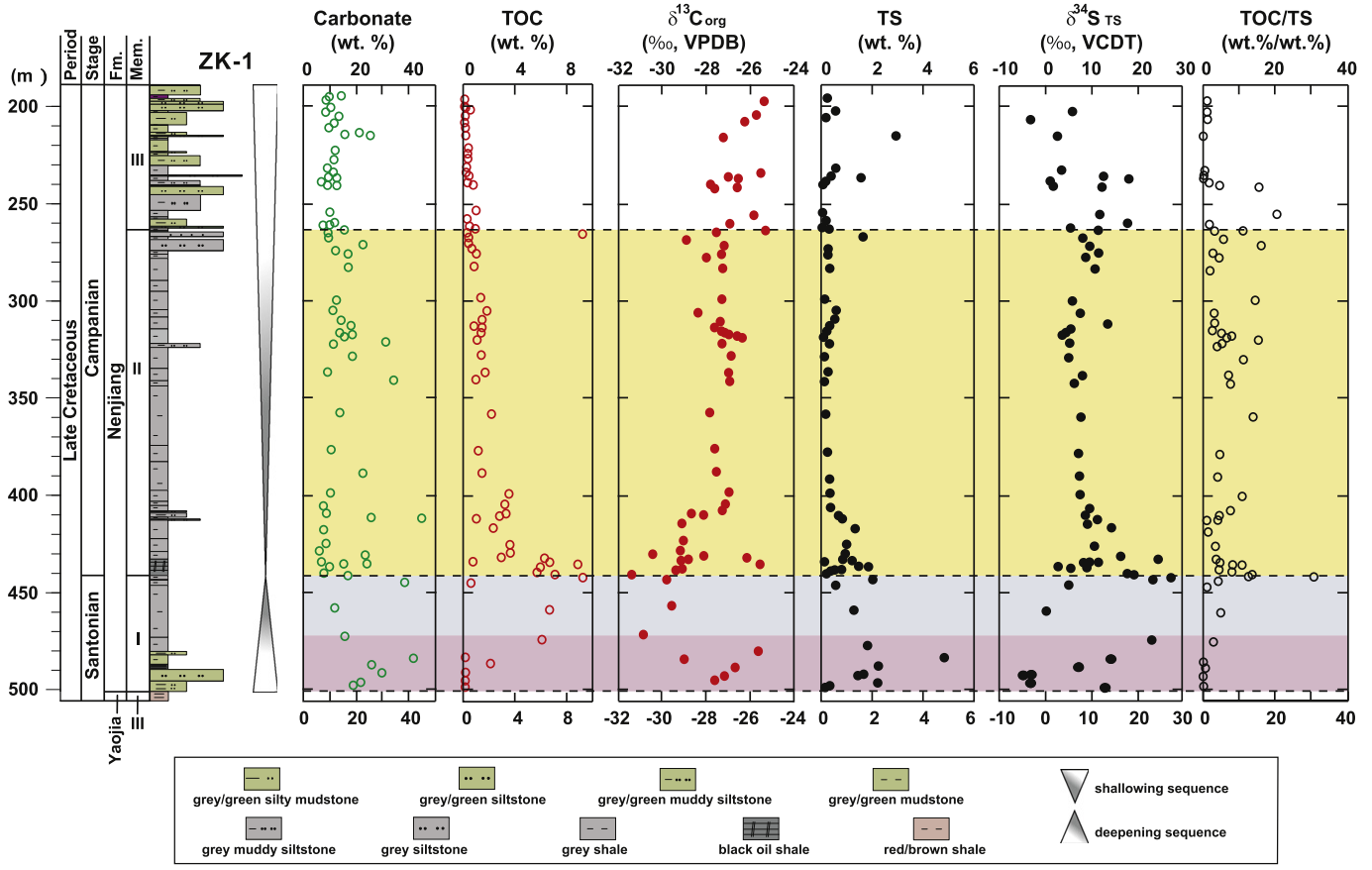

Fig. 5. Chemostratigraphy of ZK-1 core samples from the Nenjiang and Yaojia formations of the Songliao Basin in northeastern China. The shaded intervals represent interpreted water column environmental conditions (purple = euxinic/stratified, blue = anoxic/stratified, and yellow = oxygenated).

environmental factors including the availability of metabolites (i.e. organic substrates as electron donors), nutrients, and/or temperature (Habicht and Canfield, 2002; Leavitt et al., 2013; Wing and Halevy, 2014). In this case, the magnitude of fractionation is *inversely* correlated with the rate of sulfate reduction.

On the oxidative side, both heterotrophic and autotrophic microbes oxidize reduced and intermediate sulfur compounds to sulfate in order to gain energy for carbon assimilation or fixation, respectively. For example, the sulfide produced through MSR is typically re-oxidized to elemental sulfur, which is subsequently disproportionated to sulfate and sulfide, by coupling with the reduction of O_2, NO_3^-, or iron and manganese compounds (Thamdrup et al., 1993; Finster et al., 1998). Disproportionation reactions can significantly augment the fractionations induced during MSR (Canfield and Thamdrup, 1994; Canfield et al., 2010; Sim et al., 2011; Pellerin et al., 2015) resulting in isotopic contrasts between reactant sulfate and product sulfide of greater than 70‰.

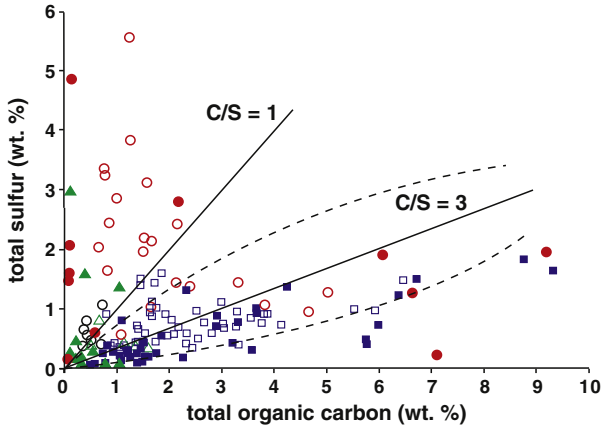

Fig. 6. Relationship of weight percent total organic carbon (TOC) to total sulfur (as pyrite) in cutting (open symbols) and core (filled symbols) from the YN-2 and ZK-1 cores, respectively, with black = Yaojia, red = Nenjiang Member I, blue = Nenjiang Member II, and green = Nenjiang Member III.

5.4. A conceptual model for the Nenjiang sulfur isotope anomaly

Considering these biological controls on the sulfur cycle and potential inputs of sulfate to the Songliao Basin, we evaluate the possible causes for the profound $\delta^{34}S$ fluctuations recorded in Nenjiang Member I. In lacustrine systems, sulfate is typically sourced from the weathering of continental rocks containing pyrite, which would have been readily oxidized if exposed beneath the Cretaceous atmosphere. Sulfate abundance in freshwater systems normally ranges between 10 and 500 μM, although, in unusual circumstances where rivers run through evaporite-rich sedimentary rocks, the concentration can reach up to 2 mM and higher (Holmer and Storkholm, 2001; Brenot et al., 2007). There are no known evaporites in the Songliao Basin or surrounding regions, so the pulsed input of sulfate from the preferential weathering of dissolved evaporites is unlikely to have been a factor in the sulfur isotope anomaly. Based on analyses of pyrite preserved in the Yaojia and upper Member II and III of the Nenjiang Formation when the system is considered to be fully lacustrine and the $\delta^{34}S$ values are invariant over long stratigraphic intervals, we estimate the sulfur isotope composition of the continental weathering input at ca. +8‰ (*cf.* Arthur et al., 1990). The invariance suggests steady state conditions where the sulfur isotope abundance of the input broadly matches that of authigenic pyrite formed in Nenjiang sediments. This would be consistent with overall low sulfate abundance in the lake at this time. In contrast, marine

incursion at the base of Nenjiang Member I would have flushed seawater sulfate with concentrations ranging from 10 to 15 mM (Berner, 2004) and $\delta^{34}S$ at +19‰ (Payton et al., 2004) into the basin.

Assuming that transgression was the proximate cause of the $\delta^{34}S$ anomaly, the sulfur isotope fractionation between dissolved sulfate in the basin waters and pyrite that accumulated in Nenjiang Member I sediments would initially *increase* to maximal values of ca. 25‰ and then *decrease* upsection to a degree that pyrite would be ^{34}S-enriched relative to seawater sulfate that initially flooded into the basin. The falling limb of the anomaly may thus be related to: (1) the rise in basinal sulfate concentrations, (2) an increase in microbial sulfur disproportionation, or (3) a decline in the rate of sulfate reduction. Given the high TS and availability of organic substrates in this interval, it is more likely that sulfate reduction rates increased rather than decreased, so option 3 does not seem viable. Options 1 and 2, however, could explain the negative $\delta^{34}S$ trend, although the magnitude of fractionation is smaller than expected if disproportionation along a strongly stratified interface was a dominant sulfur metabolism. A rise in sulfate concentration due to the connection with the marine reservoir thus appears to be the most parsimonious explanation for the negative sulfur isotope trend (*cf.* Gomes and Hurtgen, 2013).

In contrast, the rising limb of the sulfur isotope anomaly associated with an apparent decrease in fractionation may be related to either an increase in the rate of sulfate reduction, or a decrease in sulfate concentration associated with isolation of the basin from the marine reservoir and the progressive burial of pyrite. These two options may be viewed as mutually exclusive insofar as a decrease in the availability of the oxidant (sulfate) could decrease the sulfate reduction rate. Either control could explain the observed phenomenon, but we note that at its peak, the positive $\delta^{34}S$ excursion in pyrite exceeds the presumed marine sulfate input value of ca. +19‰. While it is possible that Rayleigh fractionation could drive instantaneously formed pyrite to be ^{34}S-enriched relative to the input sulfate (Bigelisen and Wolfsberg, 1958; Mariotti et al., 1981), our bulk analyses represent all of the accumulated pyrite preserved in the sediments. Thus, to explain the ^{34}S enrichments in bulk pyrite, the residual sulfate reservoir in the lake (and sediment pore waters) must also have evolved to higher ^{34}S compositions. In pore waters, residual sulfate would become progressively ^{34}S-enriched with depth, conceivably through diffusion-induced fractionation, or through MSR as either H_2S evaded upwards from the sediment due to a lack of ferrous iron, or pyrite formed due to its availability (Ferrini et al., 2010). Whether in the water column or in sediments, however, our observations are consistent with the distillation of sulfate in the lake through the burial of ^{32}S-enriched pyrite (Gomes and Hurtgen, 2013, 2015; Wu et al., 2015), but is contingent with the basin being isolated from the marine realm soon after the initial incursion.

In the ZK-1 core, however, the basal Nenjiang Member I sulfur isotope anomaly appears to be followed by a second event just beneath

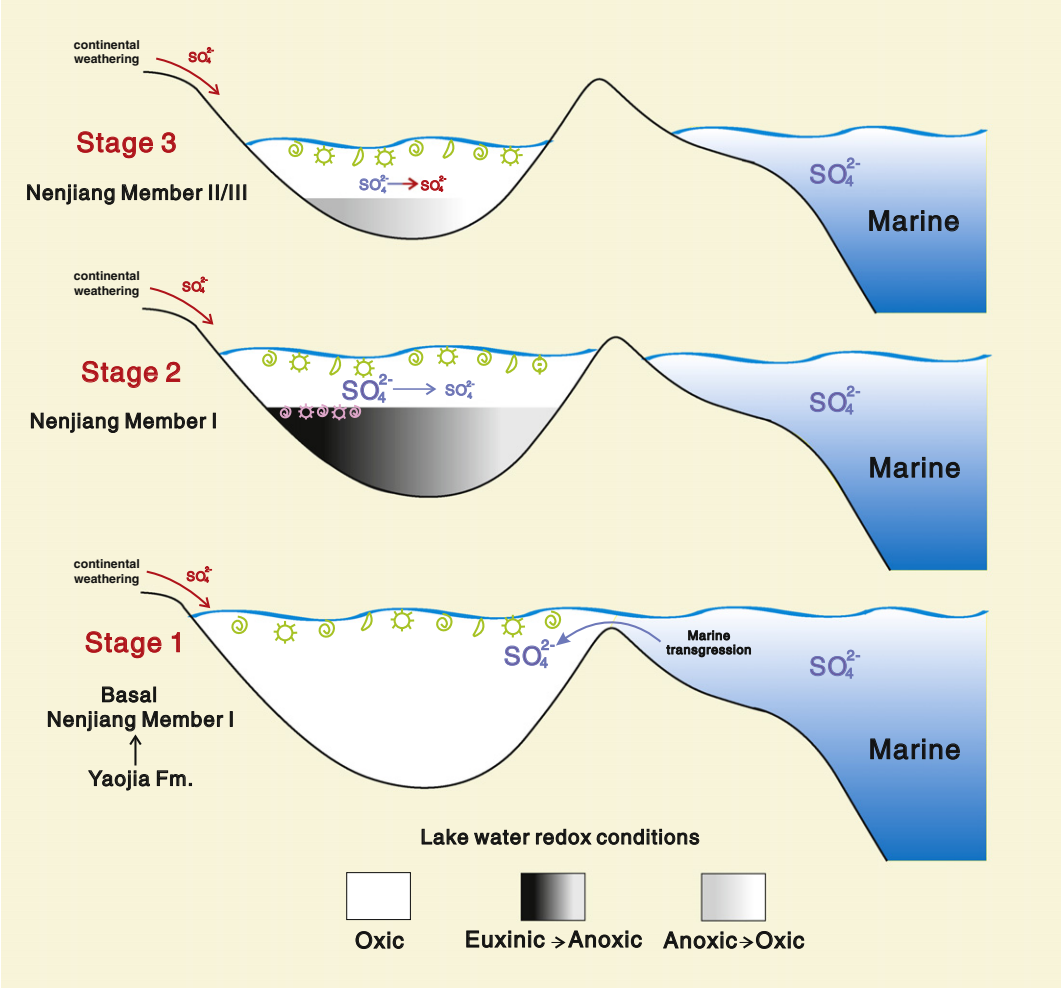

Fig. 7. The three-stage evolution of the Songliao Basin associated with marine transgression and flooding that loaded sulfate into the freshwater lake (Stage 1 = upper Yaojia and basal Nenjiang Member I). Subsequent regression and isolation of the lake resulted in the distillation of sulfate through pyrite burial and the development of euxinic conditions (that if extended to the photic zone would promote anoxygenic photosynthesis) followed by anoxic conditions as sulfate became increasingly depleted in the lake (Stage 2 = Nenjiang Member I). This stage was followed by a return to lacustrine-dominated conditions influenced by continental inputs of sulfate and coarser siliciclastics (Stage 3 = Nenjiang Members II and III).

the Santonian–Campanian boundary, and there is significant variability in $\delta^{34}S$ in Nenjiang Member III. While it is plausible that the event below the boundary represents another marine transgression into the basin, we see no evidence for rapid $\delta^{34}S$ changes in the higher resolution time-series cutting samples from the upper Nenjiang Member I in the YN-2 core. Thus, to explain the significant ^{34}S enrichment across the Member I/II transition in the ZK-1 core, we suggest that residual ^{34}S-rich sulfate in the basin (see above) was quantitatively reduced in these oil shale horizons, resulting in highly positive $\delta^{34}S$ values. In addition, the excess abundance of organic matter (up to 9% TOC) would increase the rate of MSR and thus decrease the magnitude of fractionation between residual basin sulfate and fixed pyrite in sediments (Gomes and Hurtgen, 2013, 2015; Leavitt et al., 2013). In Member III, however, the TOC is low and the sediments are coarser grained following the regional unconformity surface (Feng et al., 2010; Peng et al., 2010), suggesting that the variability in sulfur isotopes may reflect changes in the source of detrital pyrite to the lake.

Fig. 7 illustrates our conceptual environmental model for the sulfur isotope excursion in the basal Nenjiang Formation. Basin evolution through the sampled interval is divided into three stages starting with rapid marine transgression at the base of the Nenjiang (but possibly starting during deposition of the late Yaojia sediments). Sea level rise would bring high levels of sulfate to the basin thereby stimulating microbial sulfate reduction and promoting a 15‰ negative $\delta^{34}S$ shift in pyrite preserved in basal Nenjiang sediments (Stage 1), even though the lake $\delta^{34}S$ would increase because of the marine incursion. The upsection trend in Member I over the next 20 m to peak $\delta^{34}S$ values $> +25‰$ suggest that as sea level fell and the basin became restricted from marine influence, sulfate was rapidly distilled to lower concentrations with progressively higher $\delta^{34}S$ composition (Stage 2). When sulfate becomes limited by the enhanced burial of pyrite, positive $\delta^{34}S$ excursions in both residual sulfate and product sulfide would ensue (see Gill et al., 2011 for an example from the Toarcian OAE in the marine realm), at the same time that the magnitude of sulfur isotope fractionation would decrease. Stage 3 follows in the upper Nenjiang Member I prior to the Santonian–Campanian boundary where the time-series $\delta^{34}S$ trend begins its long and steady decline over ~100 m back to pre-event values. This stage would be characterized by a long-term proportional increase in the continental weathering flux of sulfate (and nutrients) to the basin, which would be expected in the early Campanian due to the extreme CO_2 levels predicted from stomatal counts on leaves and soil carbonate analyses (Quan et al., 2009; Wan et al., 2011; Hong and Lee, 2012). The step-wise decline in carbonate content at the Santonian–Campanian boundary may indicate the time of complete closure of the basin to marine inputs and pronounced decline in lake level.

6. Conclusions

The time-series elemental and sulfur isotopic profiles from the upper Cretaceous Yaojia and Nenjiang formations provide new constraints on basin evolution associated with the deposition of important source rocks in China. The sulfur isotope data is consistent with the paleontological and organic biomarker data that indicate saline and redox-stratified conditions in the depositional basin during accumulation of lower Nenjiang Member I sediments. Teleconnection with the marine realm may have been enhanced by an increase in the rate of local tectonic subsidence (Xue and Galloway, 1993) coupled to sea level rise and flooding of the Songliao Basin associated with the last of the Late Cretaceous OAEs (Haq et al., 1987; Müller et al., 2008; Friedrich et al., 2012), and may have been coupled to an increase in the rate of tectonic subsidence of the basin. This was plausibly related to higher heat flow from the mantle associated with the end of the Cretaceous Normal Superchron and beginning of rapid changes in magnetic polarity at the Santonian–Campanian boundary (Granot et al., 2012; Wan et al., 2013). The accumulation of economic source rocks in northeastern China can thus be understood in terms of the expansion of anoxic bottom waters, which would have further liberated both iron and phosphorous from sediments thereby stimulating primary productivity (Ingall and Jahnke, 1997). Organic preservation (especially associated with the peak TOC values in Nenjiang Members I and II) may also be the result of declining sulfate levels and its effect on the rate of re-mineralization of organic matter by MSR, whether the environments were marine, estuarine, or lacustrine (Smith and Klug, 1981; Holmer and Storkholm, 2001).

Acknowledgements

The authors wish to thank Laboratory Manager, Rebecca Plummer, who oversees the University of Maryland Stable Isotope Facility and who guided Cao in the analysis of samples from this study. We are also grateful for the opportunity given by the China Scholarship Council (CSC) for the one-year scholarship that allowed Cao to travel and work at the University of Maryland on this project. We thank three anonymous reviewers and the editor for their comments and suggestions on earlier iterations of this manuscript, which greatly improved its clarity and impact.

References

Arthur, M.A., Sageman, B.B., 2005. Sea-Level Control on Source-Rock Development: Perspectives from the Holocene Black Sea, the Mid-Cretaceous Western Interior Basin of North America, and the Late Devonian Appalachian Basin. In: Harris, N.B. (Ed.), The Deposition of Organic-Carbon-Rich Sediments: Models, Mechanisms, and Consequences. SEPM Special Pub Vol. 82, pp. 35–59.

Arthur, M.A., Jenkyns, H.C., Brumsack, H.J., Schlanger, S.O., 1990. Stratigraphy, Geochemistry, and Paleoceanography of Organic Carbon-Rich Cretaceous Sequences. In: Ginsburg, R.N., Beaudoin, B. (Eds.), Cretaceous Resources Events, and Rhythms: Background and Plans for Research. NATO ASI series, Series C, Mathematical and Physical Sciences 304, pp. 75–119.

Barakat, A.O., Rullkötter, J., 1997. A comparative study of molecular paleosalinity indicators: chromans, tocopherols and C20 isoprenoid thiophenes in Miocene lake sediments (NördlingerRies, Southern Germany). Aquat. Geochem. 3, 169–190.

Bechtel, A., Jia, J., Strobl, S.A.I., Sachsenhofer, R.F., Liu, Z., Gratzer, R., Püttmann, W., 2012. Palaeoenvironmental conditions during deposition of the Upper Cretaceous oil shale sequences in the Songliao Basin (NE China): Implications from geochemical analysis. Organic Geochemistry 46, 76–95.

Berner, R.A., 1982. Burial of organic carbon and pyrite sulfur in the modern ocean: its geochemical and environmental significance. Am. J. Sci. 282, 451–475.

Berner, R.A., Raiswell, R., 1983. Burial of organic carbon and pyrite sulfur in sediments over Phanerozoic time: a new theory. Geochim. Cosmochim. Acta 47 (5), 855–862.

Berner, R.A., 2004. A model for calcium, magnesium and sulfate in seawater over Phanerozoic time. Am. J. Sci. 304, 438–453.

Berner, R.A., 1984. Sedimentary pyrite formation: an update. Geochim. Cosmochim. Acta 48, 605–615.

Bigelisen, J., Wolfsberg, M., 1958. Theoretical and experimental aspects of isotope effects in chemical kinetics. Adv. Chem. Phys. 1, 15–76.

Bradley, A.S., Leavitt, W.D., Schmidt, M., Knoll, A.H., Girguis, P.R., Johnston, D.T., 2015. Patterns of sulfur isotope fractionation during microbial sulfate reduction. Geobiology 1–11.

Brenot, A., Carignan, J., France-Lanord, C., Benoît, M., 2007. Geological and land use control on $\delta^{34}S$ and $\delta^{18}O$ of river dissolved sulfate: the Moselle River Basin, France. Chem. Geol. 244, 25–41.

Canfield, D.E., Farquhar, J., Zerkle, A.L., 2010. High isotope fractionations during sulfate reduction in a low-sulfate euxinic ocean analog. Geology 38, 415–418.

Canfield, D.E., Thamdrup, B., 1994. The production of ^{34}S-depleted sulfide during bacterial disproportionation of elemental sulfur. Science 266, 1973–1975.

Crowe, S.A., Paris, G., Katsev, S., Jones, C., Kim, S.T., Zerkle, A.L., Nomosatryo, S., Fowle, D.A., Adkins, J.F., Sessions, A.L., Farquhar, J., Canfield, D.E., 2014. Sulfate was a trace constituent of Archean seawater. Science 346, 735–739.

Deng, C.L., He, H.Y., Pan, Y.X., Zhu, R.X., 2013. Chronology of the terrestrial Upper Cretaceous in Songliao Basin, Northeast Asia. Palaeogeogr. Palaeoclimatol. Palaeoecol. 385, 44–54.

Feng, Z.Q., Jia, C.Z., Xie, X.N., Zhang, S., Feng, Z.H., Timothy, A.C., 2010. Tectonostratigraphic units and stratigraphic sequences of the nonmarine Songliao Basin, northeast China. Basin Res. 22, 79–95.

Ferrini, V., Fayek, M., de Vito, C., Mignardi, S., Pignatti, J., 2010. Extreme sulphur isotope fractionation in the deep Cretaceous biosphere. J. Geol. Soc. Lond. 167, 1009–1018.

Finster, K., Liesack, W., Thamdrup, B., 1998. Elemental sulfur and thiosulfate disproportionation by *Desulfocapsa sulforexigens* sp. Nov., a new anaerobic bacterium isolated from marine surface sediment. Appl. Environ. Microbiol. 64, 119–125.

Friedrich, O., Norris, R.D., Erbacher, J., 2012. Evolution of middle to late Cretaceous oceans—a 55 m.y. record of Earth' s temperature and carbon cycle. Geology 40, 107–110.

Gao, R., He, C., Qiao, X., 1992. A new genus and species of Cretaceous dinoflagellates from two transgressive beds in Songliao Basin, NE China. Acta Palaeontol. Sin. 31, 17–29 (In Chinese with English abstract).
Gao, Y.F., Wang, P.J., Wang, C.S., 2008. Well site selecting, core profile characteristics and distribution of the speciallithology in SK-I(s). Acta Geol. Sin. 82, 669–675 (in Chinese).
Gill, B.C., Lyons, T.W., Jenkyns, H.C., 2011. A global perturbation to the sulfur cycle during the Toarcian Oceanic Anoxic Event. Earth Planet. Sci. Lett. 312, 484–496.
Goldhaber, M.B., Kaplan, I.R., 1974. The sulfur cycle. In: Goldberg, E.D. (Ed.), The Sea. Vol. 5, pp. 569–655 (Chichester, UK).
Gomes, M.L., Hurtgen, M.T., 2013. Sulfur isotope systematics of a euxinic, low-sulfate lake: evaluating the importance of the reservoir effect in modern and ancient oceans. Geology 41 (6), 663–666.
Gomes, M.L., Hurtgen, M.T., 2015. Sulfur isotope fractionation in modern euxinic systems: implications for paleoenvironmental reconstructions of paired sulfate-sulfide isotope records. Geochim. Cosmochim. Acta 157, 39–55.
Granot, R., Dyment, J., Gallet, Y., 2012. Geomagnetic field variability during the Cretaceous Normal Superchron. Nat. Geosci. 5, 220–223.
Grice, K., Schouten, S., Peters, K.E., Sinninghe-Damsté, J.S., 1998. Molecular isotopic characterization of hydrocarbon biomarkers in Palaeocene–Eocene evaporitic lacustrine source rocks from the Jianghan Basin, China. Org. Geochem. 29, 1745–1764.
Habicht, K.S., Canfield, D.E., 2002. Isotope fractionation by sulfate-reducing natural populations and the isotopic composition of sulfide in marine sediments. Geology 29, 555–558.
Habicht, K.S., Gade, M., Thamdrup, B., Berg, P., Canfield, D.E., 2002. Calibration of sulfate levels in the Archean ocean. Science 298 (5602), 2372–2374.
Habicht, K.S., Salling, L., Thamdrup, B., Canfield, D.E., 2005. Effect of low sulfate concentrations on lactate oxidation and isotope fractionation during sulfate reduction by *Archeoglobus fulgidus* strain. Appl. Environ. Microbiol. 71, 3770–3777.
Haq, B.U., Hardenbol, J., Vail, P., 1987. Chronology of fluctuating sea levels since the Triassic. Science 235, 1156–1167.
Hirst, D.M., 1974. Geochemistry of Sediments from eleven Black Sea cores. In: Degens, E.T., Ross, D.A. (Eds.), The Black Sea—Geology, Chemistry and BiologyMemoir Vol. 20. American Association of Petroleum Geologists, pp. 430–455.
Holmer, M., Storkholm, P., 2001. Sulphate reduction and sulphur cycling in lake sediments: a review. Freshw. Biol. 46, 431–451.
Holmes, J.A., Chivas, A.R., 2002. Ostracode shell chemistry—Overview. In: Holmes, J.A., Chivas, A.R. (Eds.), The Ostracoda: Applications in Quaternary ResearchGeophysical Monograph Series 131. American Geophysical Union, Washington DC, pp. 183–204.
Hong, S.K., Lee, Y.I., 2012. Evaluation of atmospheric carbon dioxide concentrations during the Cretaceous. Earth Planet. Sci. Lett. 327-328, 23–28.
Hou, D.J., Li, M.W., Huang, Q.H., 2000. Marine transgressional events in the gigantic freshwater lake Songliao: paleontological and geochemical evidence. Org. Geochem. 31, 763–768.
Huang, Y.J., Yang, G.S., Gu, J., Wang, P.K., Huang, Q.H., Feng, Z.H., Feng, L.J., 2013. Marine incursion events in the Late Cretaceous Songliao Basin: constraints from sulfur geochemistry records. Palaeogeogr. Palaeoclimatol. Palaeoecol. 385, 152–161.
Ingall, E., Jahnke, R., 1997. Influence of water-column anoxia on the elemental fractionation of carbon and phosphorus during sediment diagenesis. Marine Geology 139, 219–229.
Jia, J., Bechtel, A., Liu, Z., Strobl, S.A.I., Sun, P., Sachsenhofer, R.F., 2013. Oil shale formation in the Upper Cretaceous Nenjiang Formation of the Songliao Basin (NE China): Implications from organic and inorganic geochemical analyses. Int. J. Coal Geology 113, 11–26.
Jones, C.E., Jenkyns, H.C., 2001. Seawater strontium isotopes, oceanic anoxic events and seafloor hydrothermal activity in the Jurassic and Cretaceous. Am. J. Sci. 301, 112–149.
Leavitt, W.D., Halevy, I., Bradley, A.S., Johnston, D.T., 2013. Influence of sulfate reduction rates on the Phanerozoic sulfur isotope record. Proc. Natl. Acad. Sci. 110, 11244–11249.
Leventhal, J.S., 1983. An interpretation of carbon and sulfur relationships in Black Sea sediments as indicators of environments of deposition. Geochim. Cosmochim. Acta 47, 133–138.
Mariotti, A., Germon, J.C., Hubert, P., Kaiser, P., Letolle, R., Tardieux, A., Tardieux, P., 1981. Experimental determination of nitrogen kinetic isotopic fractionation: some principles; illustration for the denitrification and nitrification processes. Plant Soil 62, 413–430.
McKay, J.L., Longstaffe, F.J., 2003. Sulphur isotope geochemistry of pyrite from the Upper Cretaceous Marshybank Formation, Western Interior Basin. Sediment. Geol. 157, 175–195.
Müller, R.D., Sdrolias, M., Gaina, C., Steinberger, B., Heine, C., 2008. Long-term sea-level fluctuations driven by ocean basin dynamics. Science 319, 1357–1362.
Nakagawa, M., Ueno, Y., Hattori, S., Umemura, M., Yagi, A., Takai, K., Koba, K., Sasaki, Y., Makabe, A., Yoshida, N., 2012. Seasonal change in microbial sulfur cycling in monomictic Lake Fukami-Ike, Japan. Limnol. Oceanogr. 57, 974–988.
Owens, J.D., Gill, B.C., Jenkyns, H.C., Bates, S.M., Severmann, S., Kuypers, M.M.M., Woodfine, R.G., Lyons, T.W., 2013. Sulfur isotopes track the global extent and dynamics of euxinia during Cretaceous Oceanic Anoxic Event 2. Proc. Natl. Acad. Sci. 110, 18407–18412.
Payton, A., Kastner, M., Campbell, D., Thiemens, M.H., 2004. Seawater sulfur isotope fluctuations in the Cretaceous. Science 304, 1663–1665.
Pellerin, A., Bui, T.H., Rough, M., Mucci, A., Canfield, D.E., Wing, B.A., 2015. Mass-dependent sulfur isotope fractionation during reoxidative sulfur cycling: a case study from Mangrove Lake, Bermuda. Geochim. Cosmochim. Acta 149, 152–164.
Peng, G.L., Wu, C.D., Zhang, S., Chen, Y., 2010. Provenance analysis of the Member 2 and 3 of the Upper Cretaceous Nenjiang Formation in Northern Songliao Basin. Acta Sci. Nat. Univ. Pekin. 46 (4), 555–562.
Poulsen, C.J., Barron, E.J., Arthur, M.A., Peterson, W.H., 2001. Response of the mid-Cretaceous global oceanic circulation to tectonic and CO_2 forcings. Paleoceanography 16 (6), 576–592.
Prauss, M.L., 2015. Marine palynology of the Oceanic Anoxic Event 3 (OAE3, Coniacian–Santonian) at Tarfaya, Morocco, NW Africa. The transition from preservation to production controlled accumulation of marine organic carbon. Cretac. Res. 53, 19–37.
Quan, C., Sun, C.L., Sun, Y.W., Sun, G., 2009. High resolution estimates of paleo-CO_2levels through the Campanian (Late Cretaceous) based on ginkgo cuticles. Cretac. Res. 30, 424–428.
Royer, D.L., 2006. CO_2-forced climate thresholds during the Phanerozoic. Geochim. Cosmochim. Acta 70, 5665–5675.
Sachse, V.F., Littke, R., Jabour, H., Schühmann, T., Kluth, O., 2012. Late Cretaceous (Late Turonian, Coniacian and Santonian) petroleum source rocks as part of an OAE, Tarfaya Basin, Morocco. Mar. Pet. Geol. 29, 35–49.
Schenau, S.J., Passier, H.F., Reichart, G.J., De Lange, G.J., 2002. Sedimentary pyrite formation in the Arabian Sea. Mar. Geol. 185, 393–402.
Schoonen, M.A.A., 2004. Mechanisms of sedimentary pyrite formation. Geol. Soc. Am. Spec. Pap. 379, 117–134.
Sha, J.G., 2007. Cretaceous stratigraphy of northeast China: non-marine and marine correlation. Cretac. Res. 28 (2), 146–170.
Sim, M.S., Bosak, T., Ono, S., 2011. Large sulfur isotope fractionation does not require disproportionation. Science 333 (6038), 74–77.
Sinninghe-Damasté, J.S., Keely, B.J., Betts, S.E., Baas, M., Maxwell, J.R., de Leeuw, J.W., 1993. Variations in abundance and distributions of isoprenoid chromans and long-chain alkylbenzenes in sediments of the Mulhouse Basin: a molecular sedimentary record of paleosalinity. Org. Geochem. 20, 1201–1215.
Sinninghe-Damasté, J.S., Kenig, F., Koopmans, M.P., Köster, J., Schouten, S., Hayes, J.M., de Leeuw, J.W., 1995. Evidence for gammacerane as an indicator of water column stratification. Geochim. Cosmochim. Acta 59, 1895–1900.
Skelton, P.W., Spicer, R.A., Kelley, S.P., Gilmour, I., 2003. The Cretaceous World. Cambridge University Press, London (350 pp.).
Smith, R.L., Klug, M.J., 1981. Electron donors utilized by sulfate-reducing bacteria in eutrophic lake sediments. Appl. Environ. Microbiol. 42 (1), 116–121.
Song, Z.G., Qin, Y., Geroge, S.C., Wang, L., Guo, J.T., Feng, Z.H., 2013. A biomarker study of depositional paleoenvironments and source inputs for the massive formation of Upper Cretaceous lacustrine source rocks in the Songliao Basin, China. Palaeogeogr. Palaeoclimatol. Palaeoecol. 385, 137–151.
Tarduno, J.A., Brinkman, D.B., Renene, P.R., Cottrell, R.D., Scher, H., Castillo, P., 1998. Evidence for extreme climatic warmth from Late Cretaceous Arctic vertebrates. Science 282, 2241–2244.
Thamdrup, B., Finster, K., Hansen, J.W., Bak, W., 1993. Bacterial disproportionation of elemental sulfur coupled to chemical reduction of iron or manganese. Appl. Environ. Microbiol. 59, 101–108.
Wagreich, M., 2012. "OAE 3"—regional Atlantic organic carbon burial during the Coniacian–Santonian. Clim. Past 8, 1447–1455.
Wan, C.B., Wang, D.H., Zhu, Z.P., Quan, C., 2011. Trend of Santonian (Late Cretaceous) atmospheric CO_2 and global mean land surface temperature: evidence from plant fossils. Sci. China Earth Sci. 9, 1338–1345.
Wan, X.Q., Zhao, J., Scott, R.W., Wang, P.J., Feng, Z.H., Huang, Q.H., Xi, D.P., 2013. Late Cretaceous stratigraphy, Songliao Basin, NE China: SK1 cores. Palaeogeogr. Palaeoclimatol. Palaeoecol. 385, 31–43.
Wang, C.S., Feng, Z.Q., Zhang, L.M., Huang, Y.J., Cao, K., Wang, P.J., Zhao, B., 2013a. Cretaceous paleogeography and paleoclimate and the setting of SKI borehole sites in Songliao Basin, northeast China. Palaeogeogr. Palaeoclimatol. Palaeoecol. 385, 17–30.
Wang, C.S., Scott, R.W., Wan, X.Q., Graham, S., Huang, Y.J., Wang, P.J., Wu, H.C., Dean, W.E., Zhang, L.M., 2013b. Late Cretaceous climate changes recorded in eastern Asian lacustrine deposits and North American epieric sea strata. Earth Sci. Rev. 126, 275–299.
Wilkin, R.T., Arthur, M.A., 2001. Variations in pyrite texture, sulfur isotope composition, and iron systematics in the Black Sea: evidence for Late Pleistocene to Holocene excursions of the O_2–H_2S redox transition. Geochim. Cosmochim. Acta 65, 1399–1416.
Wing, B.A., Halevy, I., 2014. Intracellular metabolite levels shape sulfur isotope fractionation during microbial sulfate respiration. Proc. Natl. Acad. Sci. 111 (51), 18116–18125.
Wortmann, U.G., Bernasconi, S.M., Bottcher, M.E., 2001. Hypersulfidic deep biosphere indicates extreme sulfur isotope fractionation during single-step microbial sulfate reduction. Geology 29, 647–650.
Wu, H.C., Zhang, S.H., Sui, S.W., Huang, Q.H., 2007. Recognition of Milankovitch cycles in the natural gamma-ray logging of Upper Cretaceous terrestrial strata in the Songliao Basin. Acta Geologica Sinica-English Ed. 81 (6), 996–1001.
Wu, N., Farquhar, J., Fike, D.A., 2015. Ediacaran sulfur cycle: insights from sulfur isotope measurements ($\Delta^{33}S$ and $\delta^{34}S$) on paired sulfate-pyrite in the Huqf supergroup of Oman. Geochim. Cosmochim. Acta 164, 352–364.
Xi, D.P., Wan, X.Q., Feng, Z.Q., Li, S., Feng, Z.H., Jia, J.Z., Jing, X., Si, W.M., 2011. Discovery of Late Cretaceous foraminifera in the Songliao Basin: evidence from SK-1 and implications for identifying seawater incursions. Chin. Sci. Bull. 56 (3), 253–256.
Xue, L.Q., Galloway, W.E., 1993. Genetic sequence stratigraphic framework, depositional style, and hydrocarbon occurrence of the Upper Cretaceous QYN Formations in the Songliao Lacustrine Basin, Northeastern China. AAPG Bull. 77 (10), 1792–1808.
Ye, D.Q., Huang, Q.H., Zhang, Y., Chen, C.R., 2002. Cretaceous ostracode biostratigraphy in Songliao Basin. 11-144. Petroleum Industry Press, Beijing (in Chinese with English abstract).
Zhou, Y.S., Littke, R., 1999. Numerical simulation of the thermal maturation, oil generation and migration in the Songliao Basin, northeastern China. Mar. Pet. Geol. 16, 771–792.